Formation of a defect lattice in electroconvection of nematics

Noriko Oikawa,[1,*] Yoshiki Hidaka,[1] and Shoichi Kai[1,2]
[1]*Department of Applied Quantum Physics and Nuclear Engineering, Graduate School of Engineering, Kyushu University, Fukuoka 812-8581, Japan*
[2]*Department of Systems Life Sciences, Graduate School of Systems Life Sciences, Kyushu University, Fukuoka 812-8581, Japan*
(Received 6 April 2004; published 3 December 2004)

The formation of a defect lattice—i.e., a periodic orientational structure of numerous defect pairs—is experimentally investigated in the electroconvection of nematics. Specific twist structures of the director as a background field play an important role in the formation of a defect lattice. The observed formation sequence is as follows. With increasing applied voltage, normal rolls change into abnormal rolls due to the twisting deformation of the director. This process leads to belt-shaped domains along the abnormal rolls, in which the twist angle of the director alternates between positive and negative angles. The period of the defect lattice perpendicular to the rolls is equal to that of the domain structure in the abnormal rolls. Further increasing the applied voltage induces a secondary short-wavelength mode by the skewed varicose instability, which in turn induces defects. The periodicity of the defect lattice parallel to the rolls is due to the beating mode of the normal rolls and the secondary mode.

DOI: 10.1103/PhysRevE.70.066204 PACS number(s): 82.40.Bj, 47.20.Ky, 47.65.+a, 61.30.Gd

I. INTRODUCTION

Defects are usually formed irregularly in background-ordered structures. In some physical systems, however, ordered and uniform defects can occur. In type-II superconductors, for example, magnetic flux cores, point defects of the superconductivity state, appear ordered in a hexagonal lattice (the so-called Abrikosov vortex lattice) due to the repulsive interaction between the fluxes [1]. It is well known that this structure can be described by the Ginzburg-Landau free energy with a complex order parameter. Another example is the twist grain boundary (TGB) phase in smectic liquid crystals [2,3], where a periodic defect structure results from competition between two kinds of periodicity, such as smectic layer and twisting deformation due to molecular chirality.

For convective systems far from equilibrium, defects are commonly observed [4]. A well-known example of a periodic defect is the Eckhaus instability described by the time-dependent Ginzburg-Landau (TDGL) equation [5,6]. However, this periodic structure is not usually stationary, but is transient and finally reaches a defect-free structure [7].

In electroconvection (EHD) of nematic liquid crystals, periodic defect structures may be observed at states far from the convective onset. One example is the "defect-mediated chevron (DMC) " [8], which is observed in the dielectric and conductive regimes of homeotropic systems with weak magnetic fields. To explain the formation mechanism of the DMC, a novel theory has been proposed similar to the Turing model, in which the topological charge densities of defects and the director field are taken into account as an activator and inhibitor, respectively [9]. Another interesting example of periodic defect structures in EHD is the "defect lattice (DL)" shown in Fig. 1. The DL is closely related to oscillatory motions coupled with the director orientation and convection, and cannot be described by the simple TDGL description.

The DL was first observed two decades ago, but the formation mechanism is still unsolved [10,11]. Our recent EHD studies show that the orientational order of a nematic, as well as forming a stationary anisotropic system as a background, also dynamically couples with the convective order parameter [8]. Due to recent developments of nonlinear dynamical theory in EHD, aspects of the unsolved problems have become more clear [9,12]. In the present article, we report experimentally observed features of the transition to the DL.

II. EXPERIMENT

The experimental investigation was performed on electroconvection in the nematic liquid crystal *p*-methoxybenzilidene-*p*′-*n*-butylaniline (MBBA). The liquid crystal was filled into the space between two parallel glass plates, with a separation maintained by polymer spacers. The surfaces of the glass plates were coated with transparent electrodes (indium tin oxide), and the lateral size of

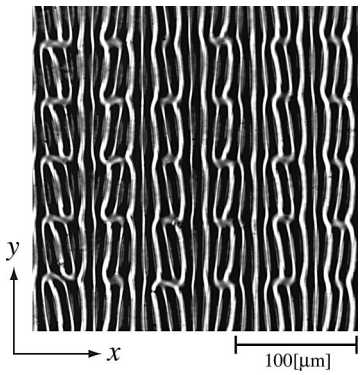

FIG. 1. Typical defect lattice pattern.

*Electronic address: oikawa@athena.ap.kyushu-u.ac.jp

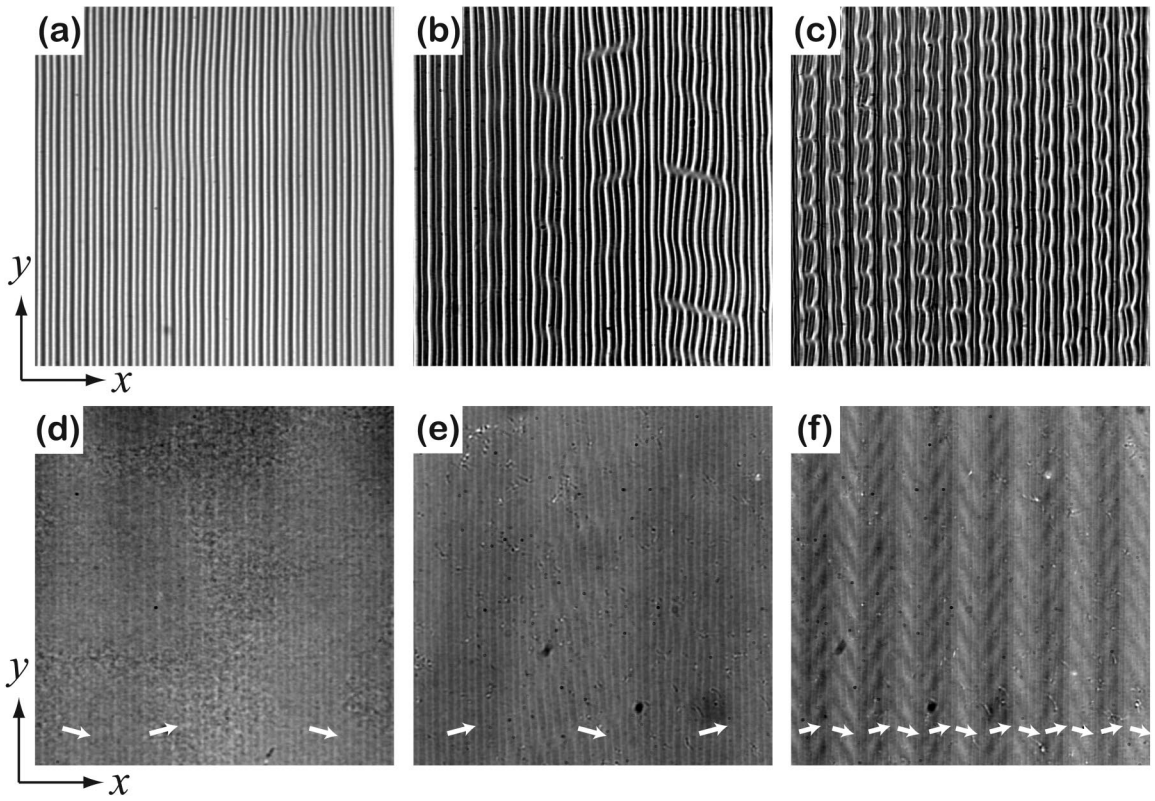

FIG. 2. Formation process of a defect lattice for increasing ε at $f=1600$ Hz in cell II. (a), (d) $\varepsilon=0.10$; (b), (e) $\varepsilon=0.26$; (c), (f) $\varepsilon=0.52$. These are convective patterns under a conventional optical system (top) and the corresponding director field images under a new optical system with a quarter-wave plate (bottom). Arrows in (d)-(f) indicate the direction of **C** in each area.

the square electrodes was 1×1 cm^2. In order to obtain uniformly planar alignment in the x-y plane parallel to the glass plates, the surfaces of the glass plates were rubbed in one direction (the x direction) after their treatment by a surfactant (polyvinyl alcohol).

The experimental temperature was kept at 30.00 ± 0.03 °C in an insulated environment with proportional-integral-differential (PID) temperature control. We used two kinds of sample cells with different material parameters. The electric conductivity was controlled by using 0.01 wt % doping of tetra-*n*-butyl-ammonium bromide (TBAB) for cell I, and 0.02 wt % doping for cell II. Cell I had a relative dielectric constant of $\epsilon_\perp=5.0$ and an electric conductivity of $\sigma_\perp=1.2\times10^{-7}\ \Omega^{-1}\,\mathrm{m}^{-1}$ at $T=30.00\pm0.03$ °C. Cell II had $\epsilon_\perp=4.7$ and $\sigma_\perp=3.2\times10^{-7}\ \Omega^{-1}\,\mathrm{m}^{-1}$. The thickness of cell I was $d=22.9\ \mu$m. Thus, the aspect ratio of the convective system in cell I was $\Gamma=437$. For cell II, $d=23.4\ \mu$m and $\Gamma=427$. The experimental results for both cells were qualitatively similar.

An ac voltage $V_{\mathrm{ac}}(t)=\sqrt{2}V\cos(2\pi ft)$ was applied to the sample in the z direction using a digital synthesizer (NF1915). Beyond a threshold voltage $V=V_c$, electroconvection occurs by the "Carr-Helfrich mechanism" [13–15] and a striped convective pattern called the Williams domain appears. Hereafter we use the normalized voltage $\varepsilon=(V^2-V_c^2)/V_c^2$.

The patterns were observed using a charge-coupled-device camera (SONY XC-75 and HAMAMATSU C4742-01) mounted on a polarizer microscope (Nikon). The observed patterns were stored on magnetic tape and magnetic disk for computer analysis. The software NIH Image and specially made software were used for the image analysis.

III. RESULTS AND DISCUSSION

A. Formation process of defect lattice

Figure 2 shows the formation process of a DL for increasing ε. A static stripe pattern, appearing in Fig. 2(a), becomes unstable and defects randomly nucleate and annihilate in space and time as shown in Fig. 2(b). This state is called

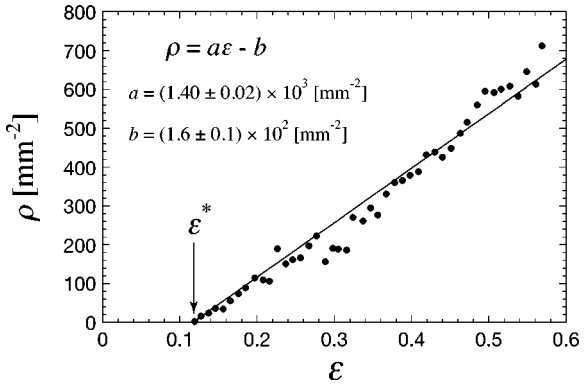

FIG. 3. Dependence of defect density ρ on ε measured at $f=800$ Hz in cell I.

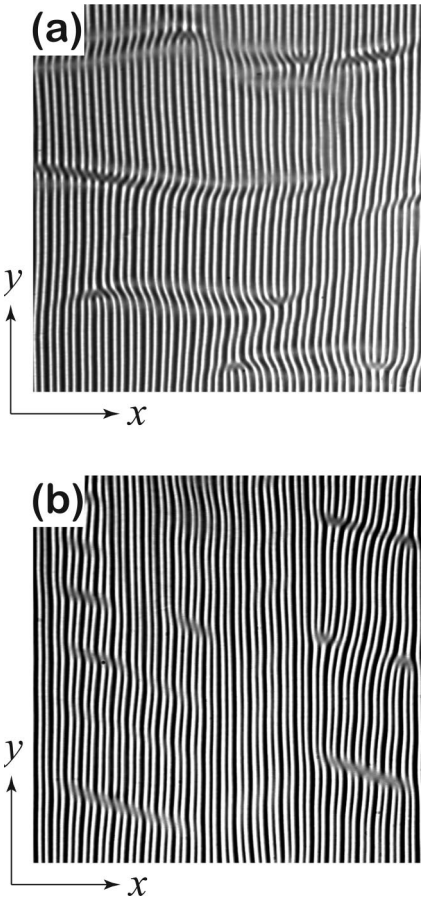

FIG. 4. (a) Conventional defect chaos and (b) defect chaos where defect motion is suppressed by the cage effect. (a) was observed at $f=100$ Hz and (b) at $f=800$ Hz in cell I. For the movies see [16].

defect chaos. The defect density linearly increases as ε increases over a threshold $\varepsilon^*=0.11$, as shown in Fig. 3. Above the threshold $\varepsilon_{\mathrm{DL}}\simeq 0.3$ for a DL, the defects are regularly ordered and the defect chaos state changes into a DL, as shown in Fig. 2(c). There is no anomaly at $\varepsilon_{\mathrm{DL}}$ on the line shown in Fig. 3.

A DL does not appear for applied frequencies below a threshold frequency f_{DL} [11]. Aspects of defect chaos states show remarkable different behavior in the regimes $f<f_{\mathrm{DL}}$ [see Fig. 4(a)] and $f>f_{\mathrm{DL}}$ [see Fig. 4(b)]. For $f<f_{\mathrm{DL}}$, defects glide over a wide area. For $f>f_{\mathrm{DL}}$ the gliding is limited, as if

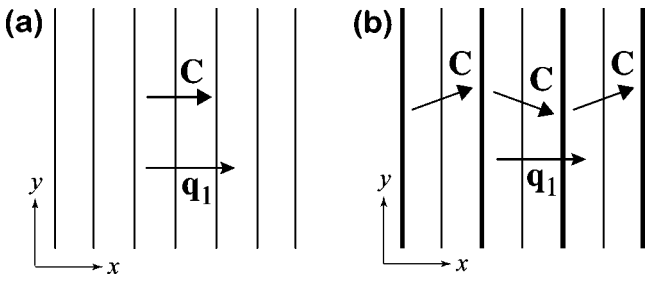

FIG. 5. Schematic presentation of (a) normal rolls and (b) abnormal rolls. The thick lines in (b) indicate the boundaries of the AR domains.

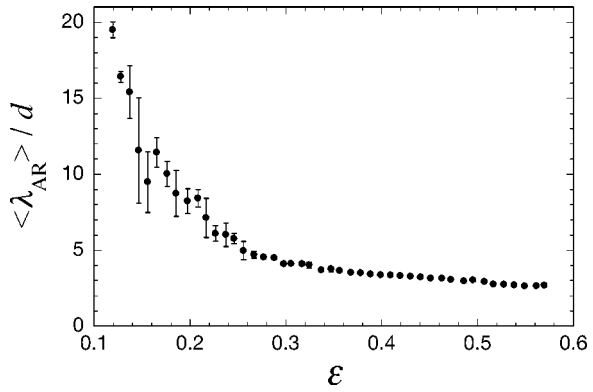

FIG. 6. Dependence of averaged width of the AR domains $\langle\lambda_{\mathrm{AR}}\rangle$ on ε at $f=800$ Hz in cell I.

there were a barrier. We call this the "cage effect," which plays an important role in the formation of a DL. f_{DL} was 650 ± 50 Hz for cell I and 1350 ± 50 Hz for cell II; the difference may result from the difference in the electric conductivity of the samples. The ratio $f_{\mathrm{DL}}/f_c=0.54$ was almost constant for both cells where f_c is the critical frequency separating the conductive regime from the dielectric one [15].

B. Abnormal rolls and cage effect

Just beyond V_c the wave vector $\mathbf{q}_1$ of the convective pattern is parallel to the **C** director which is the *x*-*y* projection of the director **n**. Both $\mathbf{q}_1$ and **C** align to *x* uniformly as shown in Fig. 5(a). This pattern is called "normal rolls" (NR). In "abnormal rolls" (AR), on the other hand, the director **C** is at an angle with *x* and is not parallel to $\mathbf{q}_1$, as schematically shown in Fig. 5(b) [17–19]. According to a recent model [12,18], the AR pattern occurs via the following mechanism. If $\mathbf{q}_1$ is parallel to **C**, the Carr-Helfrich mechanism (called hereafter *E*1) becomes most effective. On the other hand, as the flow velocity of convection increases with ε, elastic and viscous anisotropic forces of nematic liquid crystals become more enhanced. Due to these anisotropic forces, the angle between **C** and $\mathbf{q}_1$ increases by either a positive or negative value (we call this effect hereafter *E*2). When *E*2 overcomes *E*1 by raising ε, the NR become unstable. Then, **C** makes a finite angle against $\mathbf{q}_1$ (the *x* axis) and settles down to a stationary orientation, forming the AR. The AR appear from the NR through a supercritical bifurcation [12,19–21].

Ordinarily, rotation of the **C** director can be detected by crossed polarizers. In a planar system, however, **C** can be rotated only in the bulk, due to boundary anchoring with **n** parallel to the *x* axis. In the *z* direction, therefore, there is no net influence of the light polarization by the bulk rotation of **C** on polarized light transmitted through a cell. Namely, the rotation of **C** in AR cannot be observed in the conventional manner. However, one can visualize it by using a polarizer-analyzer setup with a quarter-wave plate [22]. The polarizer is set perpendicular to the *x* axis and the analyzer is set parallel to the *x* axis. The quarter-wave plate at 45° to the *x* axis is inserted between the sample and analyzer. In this method, the brightness of the images depends on the rotation angle of **C**.

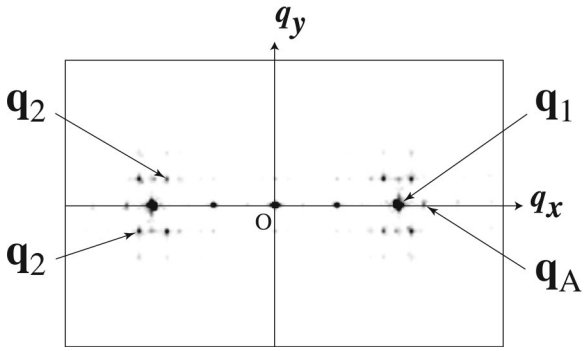

FIG. 7. Power spectrum pattern of the defect lattice shown in Fig. 1, which was observed at $f=1600$ Hz and $\varepsilon=0.55$ in cell II. The spot $\mathbf{q}_1$ corresponds to the primary convective mode, $\mathbf{q}_2$ corresponds to the secondary short-wavelength mode, and $\mathbf{q}_A$ corresponds to the abnormal rolls.

Observation of a DL using this method is shown in Figs. 2(d)–2(f), which correspond to the images (a)–(c) for the convective pattern. The direction of **C** in each domain is indicated by white arrows in Figs. 2(d)–2(f). First, wide domains with alternating brightness appear [Fig. 2(d)] which indicates AR domains. Similarly to the AR in a homeotropic system with an applied magnetic field [19,21], the clockwise and counterclockwise rotations are observed as alternate domains in the x direction. With increasing ε, the width of these domains narrow, as shown in Fig. 6, and simultaneously the domain structure becomes more periodic. The origin of this periodicity is not understood yet [23].

In the hidden twist structure, one can easily see by comparing Figs. 2(b) and 2(e) that the gliding motion of each defect is terminated at the domain boundary. That is, the cage effect is due to the domain boundary of AR. We experimentally confirmed that the optical focal length of transmitted light in the domain boundary area is shorter than that in other areas. This means that the convective amplitude as well as the distortion angle of the director increases near the domain boundary [24]. Recent theoretical research also suggests that the amplitude of convection is larger at the domain boundary of AR domains [23]. This could be due to $E1$ at the domain boundary where the director **C** is parallel to $\mathbf{q}_1$ [25]. On the other hand, as known from the definition of a defect, the convective amplitude becomes zero at a defect. It may be concluded therefore that these facts result in the cage effect.

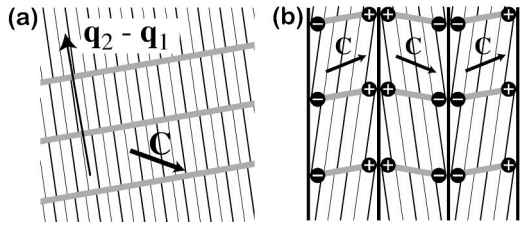

FIG. 8. Schematic presentation of (a) skewed varicose modulation and (b) defect lattice. The gray lines indicate the shear lines of rolls. The marks $\oplus$ and $\ominus$ in (b) indicate defects with positive and negative polarity, respectively. The thick lines in (b) indicate the boundaries of the AR domains.

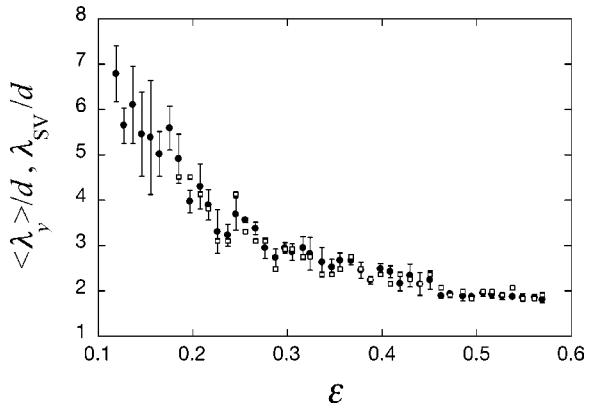

FIG. 9. Dependence of the average distance between neighboring defects in the y direction $\langle\lambda_y\rangle$ (solid circles) and the wavelength corresponding to the y component of the SV mode λ_{SV} (open squares) on ε. Measurements were made at $f=800$ Hz in cell I. λ_y was directly measured from the original pictures. λ_{SV} is obtained from the two-dimensional power spectrum of the original pictures. The $\mathbf{q}_2$ spot could be found in the power spectrum beyond $\varepsilon \simeq 0.2$.

From both the present experimental observations and theoretical research [26], it was found that below f_{DL} the domain boundaries of the AR were not parallel to the rolls, but were perpendicular. Therefore, the cage effect for defect gliding does not occur. This may be a reason why a DL does not appear below f_{DL}.

C. Creation of defects

Figure 7 shows the two-dimensional power spectrum calculated for the DL shown in Fig. 1. Secondary modes $\mathbf{q}_2$ can be observed in addition to the primary convective mode $\mathbf{q}_1$ and the abnormal roll mode $\mathbf{q}_A$. The occurrence of the short-wavelength modes $\mathbf{q}_2$ may be explained as follows. As mentioned above, the competition between the two effects $E1$ and $E2$ results in the AR pattern. That is, due to $E1$, $\mathbf{q}_1$ tends to be parallel to **C**, and due to $E2$, **C** is repulsed from $\mathbf{q}_1$. Increasing ε further, **C** prefers to rotate away from $\mathbf{q}_1$ due to a stronger $E2$. However, the large rotation of **C** is restricted by anchoring at the glass boundary. Instead, the angle

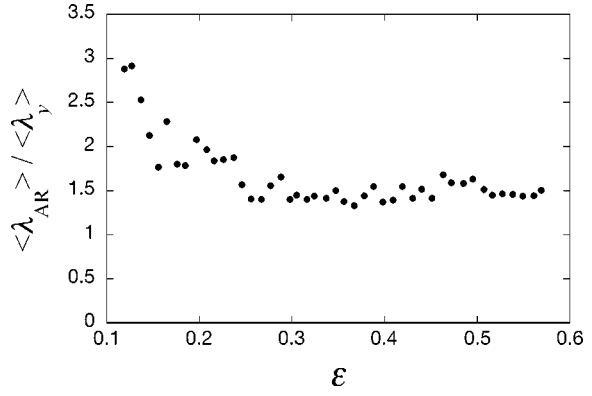

FIG. 10. Dependence of the ratio of $\langle\lambda_{AR}\rangle$ shown in Fig. 6 to $\langle\lambda_y\rangle$ on ε. Measurements were made at $f=800$ Hz in cell I.

between **C** and convective wave vector becomes larger by inducing $\mathbf{q}_2$.

The superposition of $\mathbf{q}_1$ and $\mathbf{q}_2$ may lead to a skewed varicose (SV) mode $\mathbf{q}_2-\mathbf{q}_1$ [27]. The SV modulation causes a shear displacement of rolls, as shown schematically in Fig. 8(a). The defects are nucleated by this shear and glide along it. After the gliding defects have passed, the amplitude of $\mathbf{q}_2$ becomes relatively large. If the amplitude of $\mathbf{q}_2$ grows sufficiently large, $E1$ causes the state to go back to the normal rolls, $\mathbf{q}_1$. In practice, the growth and suppression of $\mathbf{q}_2$ arise randomly in space and time, which corresponds to defect chaos.

When the width of the AR domains becomes narrow enough by raising ε, the defects cannot glide very far, due to the cage effect. In the case when the growth of $\mathbf{q}_2$ is suppressed, the stationary coexistence of $\mathbf{q}_1$ and $\mathbf{q}_2$ is realized. This coexistence state corresponds to the DL observed here [Fig. 8(b)]. In other words, in defect chaos the transient SV modulation is found, while in a DL the SV modulation is frozen by the stronger cage effect.

We measured the distance λ_y between neighboring defects in the y direction with increasing ε. As shown by the solid circles in Fig. 9, the average distance $\langle\lambda_y\rangle$ monotonically decreases. As ε increases, since $E2$ becomes stronger, $\mathbf{q}_2$ parts from $\mathbf{q}_1$ in the two-dimensional power spectrum. Therefore the wavelength $\lambda_{SV}=2\pi/(\mathbf{q}_{SV})_y$, where $\mathbf{q}_{SV}=\mathbf{q}_2-\mathbf{q}_1$, corresponding to the y component of the SV mode becomes shorter for increasing ε, as shown by the open squares in Fig. 9. The distance λ_y completely agrees with the wavelength λ_{SV}. It is clear that the defects are nucleated due to SV modulation as discussed above.

As shown in Fig. 10, the ratio of $\langle\lambda_{AR}\rangle$ to $\langle\lambda_y\rangle$ also decreases with increasing ε and becomes constant $(=1.47\pm0.07)$ beyond $\varepsilon\simeq0.3$. According to the visual observation of patterns, defect chaos changed into a DL at this point. Thus the aspect ratio of a DL is independent of ε. Furthermore it is experimentally confirmed that the ratio decreases with f/f_c.

IV. CONCLUSION

We have investigated the formation of a defect lattice in which defect pairs align periodically in the x and y directions. The hidden structures of the in-plane rotation of the director have been revealed by the use of an optical set with a quarter-wave plate.

As ε increases beyond the convective onset, the transition from normal to abnormal rolls occurs. The abnormal rolls form domain structures consisting of areas with positive and negative twist angles of the director to the x direction. We call this "pre-DL" and the periodicity of the DL in the x direction corresponds to the AR periodicity. As ε is increased further, secondary short-wavelength mode appears due to skewed varicose instability. The superposition of the secondary mode on the normal roll mode leads to the generation of defect pairs. A nucleated defect pair is confined in a domain of the abnormal rolls. Thus the periodicity of the DL in the y direction is determined from the beating mode of the superposition of the initial and secondary convective wave vectors.

In the formation process of a DL, the rotation of the **C** director originates due to the growth of the convective amplitude, but simultaneously its growth is suppressed by the planar anchoring force. The present system may be explained as being a kind of reaction-diffusion (activator-inhibitor) system, as theoretically described in Ref. [12]. According to theoretical work, Hopf and/or Turing bifurcations may occur. Based on this idea, the DL may show a limit-cycle oscillation, and the periodic domain structure inside the abnormal rolls may be a Turing pattern.

ACKNOWLEDGMENTS

The authors would like to thank W. Pesch, B. Dressel, and Y. Kuramoto for valuable discussions and comments. This work was partly supported by a Grant-in-Aid for Scientific Research (B) (Grant No. 14340123) and a Grant-in-Aid for Young Scientists (B) (Grant No. 14740239) from the Ministry of Education, Culture, Sports, Science and Technology in Japan.

[1] A. A. Abrikosov, Sov. Phys. JETP **5**, 1147 (1957).
[2] S. R. Renn and T. C. Lubensky, Phys. Rev. A **38**, 2132 (1988).
[3] T. C. Lubensky, Physica A **220**, 99 (1995).
[4] M. C. Cross and P. C. Hohenberg, Rev. Mod. Phys. **65**, 851 (1993).
[5] W. Eckhaus, *Studies in Nonlinear Stability Theory* (Springer, Berlin, 1965).
[6] Y. Hidaka, K. Hayashi, M. I. Tribelsky, and S. Kai, Mol. Cryst. Liq. Cryst. Sci. Technol., Sect. A **302**, 357 (1997).
[7] H. Yamazaki, M. I. Tribelsky, S. Nasuno, and S. Kai, in *Pattern Formation in Complex Dissipative Systems*, edited by S. Kai (World Scientific, Singapore, 1992).
[8] J.-H. Huh, Y. Hidaka, A. G. Rossberg, and S. Kai, Phys. Rev. E **61**, 2769 (2000).
[9] A. G. Rossberg and L. Kramer, Physica D **115**, 19 (1998).
[10] H. Yamazaki, S. Kai, and K. Hirakawa, J. Phys. Soc. Jpn. **52**, 1878 (1983).
[11] S. Nasuno, O. Sasaki, S. Kai, and W. Zimmerman, Phys. Rev. A **46**, 4954 (1992).
[12] E. Plaut and W. Pesch, Phys. Rev. E **59**, 1747 (1998).
[13] E. F. Carr, Mol. Cryst. Liq. Cryst. **7**, 253 (1969).
[14] W. Helfrich, J. Chem. Phys. **51**, 4092 (1969).
[15] E. Dubois-Violette, P. G. de Gennes, and O. Parodi, J. Phys. (Paris) **32**, 305 (1971).
[16] http://www.e.ap.kyushu-u.ac.jp/ap/research/EHD/Defect/DefectChaos.html
[17] H. Richter, A. Buka, and I. Rehberg, Mol. Cryst. Liq. Cryst. Sci. Technol., Sect. A **251**, 181 (1994).
[18] E. Plaut, W. Decker, A. G. Rossberg, L. Kramer, W. Pesch, A. Belaidi, and R. Ribotta, Phys. Rev. Lett. **79**, 2367 (1997).

[19] J.-H. Huh, Y. Hidaka, and S. Kai, Phys. Rev. E **58**, 7355 (1998).
[20] S. Rudroff, H. Zhao, L. Kramer, and I. Rehberg, Phys. Rev. Lett. **81**, 4144 (1998).
[21] A. G. Rossberg, N. Éber, Á. Buka, and L. Kramer, Phys. Rev. E **61**, R25 (2000).
[22] H. Amm, R. Stannarius, and A. G. Rossberg, Physica D **126**, 171 (1999).
[23] S. Komineas, H. Zhao, and L. Kramer, Phys. Rev. E **67**, 031701 (2003).
[24] K. Kondo, M. Arakawa, A. Fukuda, and E. Kuze, Jpn. J. Appl. Phys., Part 1 **22**, 394 (1983).
[25] W. Pesch (private communication).
[26] B. Dressel, Ph.D. thesis, Bayreuth, 2002.
[27] $\mathbf{q}_2-\mathbf{q}_1$ in the current study is replaced by $\mathbf{k}_{SV}$ in Ref. [11].